Submitted to NUCLEAR PHYSICS

LBL-8555
Preprint

THE $\vec{p}$ - Si ELASTIC SCATTERING IN THE REGION OF GIANT MULTIPOLE RESONANCES

C. R. Lamontagne, B. Frois, R. J. Slobodrian,
H. E. Conzett, and Ch. Leemann

December 1978

Prepared for the U. S. Department of Energy
under Contract W-7405-ENG-48

DISCLAIMER

THE $\vec{p}$ - Si ELASTIC SCATTERING IN THE REGION OF GIANT MULTIPOLE RESONANCES *

C.R. Lamontagne†, B. Frois††and R.J. Slobodrian

Université Laval, Département de Physique, Laboratoire de Physique Nucléaire, Québec, P.Q. G1K 7P4 Canada

and

H.E. Conzett and Ch. Leemann

University of California, Lawrence Berkeley Laboratory, Berkeley, California 94720 USA.

ABSTRACT : Analyzing powers and cross sections for the scattering of polarized protons from Si have been measured at eight energies between 17 and 29 MeV. The analysing powers show an "anomalous" behaviour and an optical model analysis yields a non-monotonic effect in the spin-orbit potential.

[NUCLEAR REACTIONS : $\vec{p}$ - Si scattering 17-29 MeV, measured $\sigma(\theta)$ and $A(\theta)$; derived optical model parameters.]

* Work performed under the auspices of USDOE and of AECB and NSERC-Canada.

† Presently with Département d'Informatique, Université Laval.

†† Present address : Service de Physique Nucléaire à Haute-Energie CEN Saclay, B.P. No 2,91190 Gif-sur-Yvette, FRANCE.

I - INTRODUCTION

The interest of the results reported here is twofold. Firstly, the development of a Si polarimeter[1] required precise measurements of proton polarization analyzing powers and cross sections for the scattering of silicon above 15 MeV . Secondly, the region between 15 and 30 MeV of the p - ^{28}Si system corresponds to the giant multipole resonance energies in ^{29}P [2,3].

Nuclear reaction mechanisms and the structure of nuclear states have been studied extensively via proton producing reactions such as (p,p'), (d,p), (He^3,p), (^{3}H,p), (^{4}He,p), etc. The experimental results consist predominantly of cross sections. However, when particles with spin are involved, it is well known that additional observables must be measured, for an adequate testing of theories used to interpret experiment, for the determination of relevant parameters of the reaction mechanism and the structure of the states involved. One such observable is the polarization of the outgoing proton, and to measure it a suitable polarization analyzer is required. Since yields of protons produced in nuclear reactions are inevitably low, an analyzer with good energy resolution and also with high efficiency is indicated. The conventional helium or carbon polarimeters [4,5] do not meet simultaneously both requirements. The possible usefulness of silicon detectors as proton polarization analyzers was first pointed out by Miller [6]. Recently, various reports on polarimeters using Si detectors as analyzers have been published [1,7,8].

The system described in reference 1 is intended for proton energies higher than 15 MeV, typically in the range between 15 and 30 MeV. There was thus a need for detailed experimental information as a function of energy and angle, because some existing measurements at 17 and 29 MeV [9,10] were not of sufficient accuracy and angular detail, although they permitted to forecast the usefulness of the polarimeter in this energy range. Below 15 MeV it has been shown by Hardekopf et al. [11] that there are rapid variations of the analyzing power as a function of energy, limiting somewhat the applicability as a polarization analyzer.

The energy covered by the present experiment includes the region of the giant dipole resonance in ^{29}P [3]. Other studies have been carried out in such regions for $\vec{p} + {}^{24}Mg$, $\vec{p} + {}^{27}Al$, and $\vec{p} + {}^{32}S$ [12]. Weller et al. [13,14] have studied $\vec{p} + {}^{14}C$ and $\vec{p} + {}^{56}Fe$ and they found, from phase-shift analyses of the data, that a single partial wave amplitude had the most significant energy dependence in each case. They then showed that this energy dependence was consistent with a resonance whose parameters were appropriate to those of a giant dipole resonance. It has been established through inelastic proton scattering from a broad range of nuclei that just below the giant dipole there are also quadrupole and monopole resonances [15]. The proton widths of these resonances imply that they should affect the proton elastic scattering, and should be observable provided that the shape elastic scattering described by the conventional optical model (OM) is not dominant. The scattering of protons above 10 MeV (unpolarized and polarized) from nuclei heavier than helium has been traditionally analyzed by the OM with varying degrees of sophistication [16,17,18], and the resulting para-

meters and wave functions are extensively used in the distorded wave Born approximation (DWBA) calculations of nuclear reactions [19]. However, experimental data and corresponding OM parameters are available at rather widely spaced energy intervals, and in applications a monotonic variation with energy is assumed to provide the necessary interpolations or extrapolations. However, the validity of the latter and of the resulting wave functions may be seriously affected by resonances in general and, in particular, by the giant resonances present in nuclei. The region of the giant dipole resonance for ^{29}P is located near 20 MeV in the $^{28}Si+p$ channel, and the evidence for quadrupole and monopole resonances in other nuclei would centre them about 2 MeV lower in energy [15].

II - EXPERIMENTAL DETAILS AND RESULTS

The polarized proton beam facility of the Berkeley 88-inch cyclotron[20] was used to measure relative cross sections and asymmetries in the scattering from Si at 2 MeV intervals from 17 to 29 MeV inclusive. The natural Si target (92.2% of ^{28}Si) was prepared from crystalline high purity material, and the thickness was determined to be 6.5 ± 0.2 mg cm^{-2} using a method of α-particle transmission using a source of ^{241}Am. Although ref. 20 contains most of the details of the standard experimental procedure, a brief summary is presented here for completeness. Figure 1 shows the layout of the scattering chamber, detectors and polarimeter.

The incident beam energy was determined by momentum analysis through a 110° bending magnet. The centre of the target energies were calculated from such determinations and the measured target thickness quoted above. The beam alignment was monitored continuously with a split Faraday cup, requiring only minor corrections during the experiment. The beam polarization was measured with a helium polarimeter, placed following the scattering chamber. It consisted of a gas cell and a pair of ΔE-E counter telescopes set at opposite sides of the beam. The protons scattered from helium were detected at angles corresponding to maximum analyzing efficiency that is 114° to 117° for energies of 25 MeV or higher, and 75.6° for energies below 25 MeV. The analyzing power of helium was known with great detail from recent accurate measurements [20]. Typical beam polarizations were between 75 and 85%. Each asymmetry measurement was accompanied by a simultaneous beam polarization measurement. Four pairs

of silicon detectors placed at symmetrical angles with respect to the beam were used for the asymmetry measurement, spanning an angular range of 30^{o} at 10^{o} intervals. In order to correct for geometrical effects each angle was measured with two spin orientations of the polarized beam. The spin reversal was simply accomplished at the ion source reversing the current through a solenoid [21]. The relative efficiencies of the eight detector systems used during the experiment were determined with an unpolarized beam, under identical conditions, by switching off the radio-frequency transition in the ion source, and measuring the same laboratory angle with the four detector pairs in succession.

A schematic diagram of the electronics is shown in figure 2. Pulses from the eight detectors were mixed and routed to 256 channel sections of a Nuclear Data 4096 channel analyser. A typical run consisted of the yield of the eight detectors for one spin orientation, stored in 2048 channels, and also for the other spin orientation, stored in the remaining 2048 channels. The data of a complete run were transferred to Dec-tape by means of a PDP-5 computer. For all energies except 25.25 MeV measurements were confined between 15^{o} and 54^{o}. At 25.25 MeV a full angular distribution was measured, which has been published elsewhere [22] in relation to the ground state rotational band of ^{28}Si. Figure 3 shows some typical spectra, and the data reduction was straight-forward. A first reduction was performed during the experiment as described by Plattner et al. [23], and a second, definitive one, was performed at Université Laval using a PDP-15 computer. The analyzing power is given by

$$A = \frac{1}{P_b} \frac{r-1}{r+1} \qquad (1)$$

with $$r = \left(\frac{L_{\uparrow} R_{\downarrow}}{R_{\uparrow} L_{\downarrow}}\right)^{1/2} \quad (2)$$

L and R are yields, P_b is the beam polarization and A is the analyzing power of the scatterer, the arrows indicate the direction of polarization of the beam relative to the scattering plane. A simultaneous measurement of asymmetries from ^{4}He and Si permits the determination of the analyzing power of the latter. Errors of the calculated asymmetries are due to statistical fluctuations, to the uncertainty of the scattering angle, and to the error in the measurement of the beam polarization. The cross sections were calculated from the yields $L_{\uparrow}$, $R_{\uparrow}$, $L_{\downarrow}$, $R_{\downarrow}$ with a code written in FOCAL language for the PDP-15 computer. The errors of the calculated cross sections are due to the same first two sources mentioned above for the polarizations, and also to the target thickness uncertainty, to the error in the relative normalization of the four pairs of detectors and to the charge collection uncertainty. The absolute normalization of cross sections was carried out by calibration of the split Faraday cup located behind the helium polarimeter, using a removable one that can be placed at the exit of the scattering chamber (see Fig. 1). Two additional monitor detectors and also the helium polarimeter counts permitted a consistency check of the cross section normalizations. Figure 4 shows comprehensive graphs of cross sections and polarizations, and tables I and II give their numerical values and errors.

III - OPTICAL MODEL ANALYSIS AND SEARCH ON THE p-WAVE PHASE SHIFTS

The cross section and polarization data were analyzed first with the code Seek due to Melkanoff, Sawada and Raynal [12]. The parametrisation is made in terms of a potential

$$V = V_{coul}(r) + V_{cr}(r) + iV_{ci} + [V_{sr}(r) + iV_{si}(r)]\,\hbar^2(\vec{s}.\vec{l}) \qquad (3)$$

$$V_c(r) \begin{cases} = \dfrac{ZZ'e^2}{2r_c}\left(3 - \dfrac{r^2}{r_c^2}\right) & \text{for } r \le r_c \\ = \dfrac{ZZ'e^2}{r} & \text{for } r > r_c \end{cases}$$

$$r_c = R_c\, M_t^{1/3}$$

Ze and Z'e are respectively the charges of the target and of the projectile.

$$V_{cr}(r) = -\,V/\left(1 + \exp\frac{r-r_r}{a_r}\right) \qquad (4)$$

where

$$r_r = R_r M_t^{1/3}$$

$$V_{ci}(r) = -\,W/\left(1+e^{\frac{r-r_i}{a_i}}\right) - W_D \exp\left[-\left(\frac{r - r_i}{b}\right)^2\right] \qquad (5)$$

with

$$r_i = R_i M_t^{1/3}$$

A Thomas form spin-orbit term is used :

$$\frac{\hbar^2}{2}\left[V_{sr}(r) + iV_{si}(r)\right] = 2(V_s + i\,W_s)\,\frac{1}{r}\frac{d}{dr}\,\frac{1}{1+e^{(r-r_r)/a}} \qquad (6)$$

The programme minimizes x_T^2 defined as

$$\chi_T^2 = \chi_\sigma^{\,2} + \chi_P^2 = \sum_i \left[\frac{\sigma_{th}(\theta_i) - \sigma_{exp}(\theta_i)}{\Delta\sigma_{exp}(\theta_i)}\right]^2 + \sum_j \left[\frac{P_{th}(\theta_j) - P_{exp}(\theta_j)}{\Delta P_{exp}(\theta_j)}\right]^2$$

After an extensive search using this code (SEEK) it became apparent that it was difficult to arrive at an acceptable fit to the data. The spin-orbit diffuseness parameter in this code is kept equal to that of the real central potential. However, according to Satchler [24] a spin-orbit parameter smaller than that of the real potential is preferable. Thus it was decided to try the code MAGALI [25] which allows the use of independent geometrical parameters, and also enables the use of either a gaussian or a Saxon-Woods derivative form factor for the surface absorption. The latter was used consistently in the work reported here. Table III contains the parameters corresponding to "best fits" of the experimental data (solid lines shown on figure 4). Figure 5 is a plot of the relevant dynamical parameters : V, V_{so}, W_d and W, showing a strong non monotonic behaviour of V_{so}. A similar trend is also shown by W and W_D, but it is difficult to attach much significance to it because their sum is essentially independent of energy, and the quality of the fits depends on the sum and only weakly on the separate values

of W and W_D. They do show a shift from volume to surface absorption in this energy region. The distinctly poorer quality of fits obtained when V_{so} is interpolated linearly between 17 and 29 MeV is illustrated in table IV. As expected, the deterioration of the fits to the polarization data, as shown by the large increases in χ^2_P, is the most marked.

Since the standard OM calculation does not include contributions to the scattering from other than the shape-elastic resonances, it is possible that the anomalous behavior found for $V_{so}(E)$ is due to a giant resonance contribution to the scattering which is not specifically included in the calculation. In their investigations over the giant resonance regions of ^{15}N and ^{57}Co via $\vec{p} + {}^{14}C$ and $\vec{p} + {}^{56}Fe$ elastic scattering, Weller et al.[13,14] carried out phase shift analyses of their data, and they found, in each case, an energy dependence of a single partial-wave amplitude that showed a broad resonance behavior which they interpreted to be consistent with the effect of a giant dipole resonance. Weller and Divadeenam [26] had, also, examined the phase shifts derived from the OM analysis of our data [3], and they concluded that the $g_{9/2}$ partial wave exhibited an energy dependence appropriate to a $J^\pi=9/2^+$ resonance at E_{LAB} = 23 MeV, with a proton width of 1.62 MeV and a total width of 6.0 MeV. This clearly had no connection with the giant dipole resonance in ^{29}P, which is restricted to $J^\pi=1/2^-$ or $3/2^-$ components since only these

can decay to the $1/2^+$ ground state via an E1 transition. Then, on the basis of a 2p-1h doorway state calculation, they concluded that a strong $9/2^+$ resonance, with an energy and a width appropriate to account for the data, was indeed predicted by the calculation.

We find an alternate more plausible explanation for the behavior of the $g_{9/2}$ phase shifts in $\vec{p} + {}^{28}Si$ scattering between 17 and 29 MeV, and we raise the question as to whether or not the resonance behavior seen in the $\vec{p}+{}^{14}C$ and the $\vec{p} + {}^{56}Fe$ studies [13,14] can be attributed unambiguously to the giant dipole resonances of those systems.

Table V contains the phase shifts corresponding to the best fit OM parameters of Table III, and table VI has those corresponding to the OM parameters of Table IV, where V_{so} was interpolated linearly between 17 and 29 MeV with the other parameters adjusted to provide the best fit to the data. Figure 6 shows the energy dependence of phase shifts of particular interest, the p and g-waves. It is seen that the main effect of the larger spin-orbit strength is the expected larger g-wave spin-orbit splitting due to the surface-peaked nature of V_{so}. In order to examine the resonance-like nature of the partial-wave amplitudes,

$$f_{\ell j} = [\eta_{\ell j} \exp(2i\delta_{\ell j}) - 1] / 2i \quad , \qquad (7)$$

we have plotted their Argand diagrams in Fig. 7. It is seen that the anomalous behavior of V_{so} (Table III) does not result in a resonant behavior of $f_{g\ 9/2}$ between 17 and 29 MeV which is not already present for the potential with the linearly interpolated V_{so}, i.e. a shape elastic effect. It is, also, not clear that the energy dependence

of $f_{g\ 9/2}$ can be described as resonant. Its trajectory certainly does not trace an approximate circle in a counter-clockwise direction [27], and the resonance-like nature of $\eta_{g\ 9/2}$ in Fig. 6 is entirely due to the passage of $f_{g\ 9/2}$ close to the centre of the unitary circle for E_{LAB} near 22 MeV. Thus, the ascription of the $g_{9/2}$ phase shifts of Table V to a doorway state resonance is questionable. In order to investigate whether the giant dipole resonance of ^{29}P was in some way connected with the anomalous behaviour of $V_{so}(E)$ in our own analysis, we performed a constrained phase-shift analysis of our data. That is, we searched on the p-wave phase shifts while constraining the other phase shifts to their OM values for the potential with the linearly interpolated values of $V_{so}(E)$. The p-wave amplitudes determined in this manner were less smooth functions of energy than those shown in Fig. 7, but their general trends were similar. Thus, no evidence for a p-wave resonance was found, and therefore a straightforward effect due to the ^{29}P giant dipole resonance is not seen in our partial wave analysis.

We note that the behavior of $f_{g\ 9/2}$ in Fig. 7 is qualitatively similar to that of $f_{d_{5/2}}$ from the phase shift analysis of the $\vec{p}$ + ^{56}Fe data [14]. That is, the $f_{d_{5/2}}$ trajectory also passes very near to the center of the unitary circle at "resonance" without tracing an approximate circle in the proper direction [28,29]. Even though it was found in ref. 14 that the gross features of the energy dependence of the cross-section and the analyzing power were reproduced in an OM analysis the fact that the strongest energy dependence of the phase shifts was

contained in the single $d_{5/2}$ partial wave was cited as evidence for a single $5/2^+$ state consistent with the giant dipole resonance of ^{57}Co. However, as is shown in Fig. 6, the most significant energy dependence in our $\vec{p}$ + ^{28}Si case is contained in the single $g_{9/2}$ partial wave, which we know to be due to the shape-elastic potential scattering of that particular partial wave. An examination of Fig. 4 of ref. 14 shows that the $d_{3/2}$ phase-shift behavior is quite similar to the $d_{5/2}$, but displaced about 2 MeV to lower energy. Although this was discussed briefly in ref. 14, it seems inconsistent to describe the $d_{5/2}$ phase-shift behavior to a $5/2^+$ resonance while not arguing similarly for the existence of a $3/2^+$ resonance, also.

Since, it has been noted [28] that proton OM calculations for nuclei near mass number 50 show the d-wave amplitudes to be characterized by $\eta \simeq 0$ near 10 to 15 MeV, it is important to try to rule out shape-elastic scattering as the origin of the resonance-like behavior of the $d_{3/2}$ and $d_{5/2}$ phase shifts in the analyses of the $\vec{p}$ + ^{14}C (ref.13) and $\vec{p}$ + ^{56}Fe (ref. 14) data, respectively. This question can be pursued more readily for p + nucleus systems where the entrance channel energy corresponding to the giant dipole resonance is such that the J^π of the shape-elastic resonance effect is different from that of the giant resonance. This is the case in our $\vec{p}$ + ^{28}Si studies, and we are currently extending the investigation to neighboring nuclei.

In view of the collective nature of the giant dipole resonance [30], the lack of success in finding any evidence for a p-wave resonance in our partial wave analysis is not surprising. Such a resonance would correspond to the excitation of a single valence proton in ^{29}P, whereas most of the dipole strength should be found in the collective two particle one hole (2p-1h) excitations [31]. In addition, an isospin splitting of the giant dipole resonance (GDR) in nuclei with ground state iso-spin $T_0 \neq 0$ has been predicted [32,33] with the $T_> = T_0 + 1$ component located several MeV above the $T_< = T_0$ component. For the small value of $T_0 = \frac{1}{2}$, most of the strength should be concentrated in the $T_> = \frac{3}{2}$ state [32], and this major component would then not couple directly to the $T = \frac{1}{2}$ $p + ^{28}Si$ elastic channel. Calculated photonuclear cross sections for ^{13}C and ^{17}O demonstrate this iso-spin splitting and agree with the available data [31]. Other effects in the giant dipole region will appear diluted over many partial waves in the pure single particle representation of the underlying continuum.

Very recently, Weller et al. [34] have studied $\vec{p} + ^{13}C$ elastic scattering in the region of the GDR, and although some broad resonances 1^- and 2^- appear in their phase shift analysis, possibly related to the GDR, their conclusion is that there is no clear correlation, in agreement with our own appraisal of the situation. Further experimental and theoretical studies are clearly necessary.

Other possibilities for an explanation of the anomalous behavior of V_{SO} between 17 to 29 MeV are suggested by the recent work of Mackintosh and his collaborators on the proton OM potential [35-37]. They pointed

out that there can be substantial contributions to both the real and imaginary parts of the potential from the coupling to deuteron, i.e. neutron pickup, channels. In fitting quite precise $\vec{p}$ + ^{40}Ca elastic scattering data at 30.3 MeV with a coupled reaction channel (CRC) calculation, they found a substantial difference in the proton V_{so} as compared to that from an OM fit. If one considers the proton potential which fits the data in the CRC calculation as a "bare" potential, which does not include the deuteron effects implicitly it is possible that the varying $V_{so}(E)$ strength we find in the OM analysis of our $\vec{p}$ + ^{28}Si data is a reflection of the substantial coupling to the deuteron channels that is evidenced by the large spectroscopic factors for ^{28}Si(p,d) transitions to low-lying states of ^{27}Si [38,39]. Further alternatives are suggested by two very interesting recent developments with respect to proton OM potentials. The first is the finding that a phenomenological representation of the pickup-channel coupling effects results in an ℓ-dependent OM component [36], the inclusion of which provided a significantly improved fit to the p + ^{40}CA differential cross-section angular distribution. The second is the observation that there is a theoretically expected need for an imaginary spin-orbit term in the OM potential. The inclusion of such a term then provides a much improved fit to the $\vec{p}$ + ^{40}Ca analyzing power data [37].

IV - CONCLUSIONS

A standard OM analysis of our 17 to 29 MeV $\vec{p}$ + ^{28}Si cross section and analyzing-power data yields an anomalous energy dependence of the spin-orbit strength $V_{so}(E)$ which is correlated with the giant dipole resonance region of ^{29}P. An examination and comparison has been made of the phase shifts from : a) the best fit OM potential $V_{so}(E)$, b) a linearly interpolated $V_{so}(E)$, and c) a constrained phase shift analysis. We conclude from this comparison that there is no evidence that the energy dependence of $V_{so}(E)$ is caused by the coupling of the giant dipole resonance to a single particle continuum state of the elastic channel, and we suggest that the previously reported evidence for such an effect in $\vec{p}$ + ^{14}C and $\vec{p}$ + ^{56}Fe elastic scattering is not conclusive.

It seems clear that the recently established grounds for ℓ-dependent central and imaginary spin-orbit OM interactions may require the inclusion of such terms [36,37]. Their inclusion in an OM analysis of our data would, most likely, result in an altered behavior of $V_{so}(E)$.

We are in complete accord with the remarks of ref. 37 concerning the importance of precise proton elastic scattering data over sufficient energy and mass ranges in order to establish the behavior of specific terms of the OM potential such as the ℓ-dependent central term, and both the real and imaginary spin-orbit interactions. All that has been lacking in the recent past has been the motivation to

do so, because the presently available polarized-beam facilities have certainly simplified the experimental task. We are currently pursuing such an experimental program.

Similar considerations apply to the elastic particle-nucleus interaction projectiles other than protons and should be investigated in the region of giant multipole resonances using polarized beams.

V - ACKNOWLEDGEMENTS

Some of the authors (C.R.L., B.F, and R.J.S.) would like to gratefully acknowledge the generous hospitality of L.B.L.
Many thanks are due to the CTI of Université Laval for the use of its computing facilities. The cooperation of the 88" cyclotron staff was essential to the success of the work and we express our warmest gratitude.

FIGURE CAPTIONS

FIG. 1 - Schematic view of the scattering chamber, helium polarimeter, detectors and Faraday cup.

FIG. 2 - Block diagram of the electronics.

FIG. 3 - Sample spectra showing excellent separation between the ground state and first excited state.

FIG. 4 - Graph of cross sections and polarizations from tables I and II. Notice the rapid variation of polarizations as a function of energy. The solid lines correspond to optical model fits with the parameter of table III.

FIG. 5 - Graph of the strength parameters V, V_{so}, W_d and W of table III as a function of energy. The scale of parameter V is at the left. All the others are to be read on the scale at the right.

FIG. 6 - a) Optical model p-wave phase shifts. The dots are from the best-fit V_{so} (table V) and the triangles are from the linearly interpolated V_{so} (Table VI)

b) Optical model g-wave shifts. The symbols have the same meaning as in a).

FIG. 7 - Argand diagrams of p and g wave amplitudes, (eq.7). The solid lines are the trajectories obtained with best-fit V_{so} (Table IV) the dashed lines with the linearly interpolated V_{so} (Table IV). The proton energy is indicated along the curves. The centre of the unitary circle is at the point (0,0.5).

REFERENCES

1.- B. Frois, J. Birchall, R. Lamontagne, R. Roy and R.J. Slobodrian, Nucl. Instr. and Meth. 96 (1971) 431 and Refs. Therein.

2.- M. B. Lewis and F.E. Bertrand, Nucl. Phys. A196 (1972) 337;
M. B. Lewis, Phys. Rev. Letters 29 (1972) 1257;
G.R. Satchler,Nucl. Phys. A195 (1972); particles and Nuclei.

3.- C.R. Lamontagne, B. Frois, R.J. Slobodrian, H.E. Conzett, Ch. Leemann, R. de Swiniarski, Phys. Lett. 45B, (1973) 465.

4.- G.J. Lush, T.C. Griffith and D.C. Imrie, Nucl. Instr. and Meth 27 (1964) 229.

5.- C. Tschalär, C.J. Batty and A.I.Kilvington, Nucl. Instr. and Meth. 78 (1970) 141.

6.- D.W. Miller, Proc. Int'l. Symp. on Polarisation Phenomena of Nucleons (eds. P. Huber and H. Schopper; Birkäuser, Basel 1966).

7.- J.P. Martin and R.J. A. Levesque, Nucl. Instr. and Meth. 84, (1970) 211.

8.- J. Birchall, H.E. Conzett, W. Dahme, J. Arvieux, F.M. Rad, R. Roy. R.M. Larimer, Nucl. Instr. and Meth. 123 (1975) 105.

9.- D.J. Baugh, C.W. Greenlees, J.S.Lilley and S. Roman, Nucl. Phys. 65 (1965) 33.

10.- R.M. Craig et al., Nucl. Phys. 83 (1963) 493.

11.- R.M. Hardekopf, D.D. Armstrong and P.W. Keaton Jr. Nucl. Instr. and Meth. (1972).

12.- J. Birchall, H.E. Conzett, C.R. Lamontagne, R.M. Larimer, R. Roy and R.J. Slobodrian, LBL-2366 (1973) (Unpublished).

13.- H.R. Weller, N.R. Robertson, D. Rickel and D.R. Tilley, Phys. Rev. Lett. 33 (1974) 657.

14.- H.R. Weller, J. Szücs, J.A. Kuehner, G.D. Jones, and D.T. Petty, Phys. Rev. C13 (1976) 1055.

15.- M.B. Lewis and F.E. Bertrand, Nucl. Phys. A196 (1972) 337
M.B. Lewis, Phys. Rev. Lett. 29 (1972) 1257.
G.R. Satchler, Nucl. Phys. A195 (1972) 1; Particles and Nuclei 5, (1973) 105.

16.- P.E. Hodgson, Ann. Rev. of Nucl. Science 17 (1967) 1 and Refs. therein.

17.- F.D. Bechetti Jr. and J.W. Greenlees, Phys. Rev. 180 (1969) 1190.

18.- F. Perey in Polarization phenomena in nuclear reactions, eds. H.H. Barschall and W. Haeberli (University of Wisconsin Press. Madison 1971) and Refs therein.

19.- N. Austern, Direct Interaction Theories, John Wiley and Sons (1970) and refs. therein).

20.- A.D. Bacher et al., Phys. Rev. C5 (1972) 1147.

21.- D.J. Clark, A.U. Luccio, F. Resmini and H. Meiner, Proceedings of the Fifth International Cyclotron Conference, 1969 (Butterworth, London, England, 1971) p. 610.

22.- R. de Swiniarski, H.E. Conzett, C.R. Lamontagne, B. Frois and R.J. Slobodrian, Can. Jour. of Phys. 51, (1973) 1293.

23.- G.R. Plattner, T.B. Clegg and L.G. Keller, Nucl. Phys. A111 (1968) 481.

24.- G.R. Satchler, Nucl. Phys. A92 (1969) 273.

25.- J. Raynal, 1969 D.Ph. T169, 42 (CEN Saclay).

26.- H.R. Weller and M. Divadeenam, Phys. Lett. 55B (1975) 41.

27.- R.H. Dalitz, Ann. Rev. Nucl. Sci. 13 (1963) 339.

28.- W. Haeberli, Phys. Rev. C14 (1976) 2322.

29.- H.R. Weller, Phys. Rev. C14, (1976) 2324.

30.- D. Rowe, Nuclear Collective Motion, Methuen and Co. Ltd (1970) and refs. therein.

31.- D.J. Albert et al., Phys. Rev. C16, 503 (1977).

32.- S. Fallieros, B. Goulard, and R.H. Venter, Phys. Lett. 19 (1965) 398.

33.- B. Goulard and S. Fallieros, Can.J. Phys. 45 (1967) 3221.

34.- H.R. Weller, J. Szücs, P. G. Ikossi, J.A. Kuehner, D.T. Petty, R.G. Seyler, Phys. Rev. C18 (1978) 1120.

35.- R.S. Mackintosh and A.M. Kobos, Phys. Lett. 62B (1976) 127.

36.- R.S. Mackintosh and L.A. Cordero, Phys. Lett. 68B (1977) 213.

37.- R.S. Mackintosh and A.M. Kobos, J. Phys. G to be published.

38.- C.D. Jones, R.R. Johnson, and R.J. Griffiths, Nucl. Phys. A107 (1968) 659.

39.- R.L. Kozub, Phys. Rev. 172 (1968) 1078.

TABLE I. CROSS SECTION IN MB SR^{-1}, ANGLES ARE IN DEGREES AND ENERGIES IN MEV.

θ_{CM} \ E_{LAB}	17.13		19.04		20.84		22.99		24.93		27.14		28.98	
15.53	2013	± 75	1937	± 113	2012	± 79	1727	± 92	1708	± 30	1593	± 44	1570	± 29
17.60	1622	138	1450	113	1523	74	1378	43	1565	79	1225	88	1433	44
19.67	1187	69	1075	52	1210	90	1120	110	1223	53	1019	200	1142	20
21.74	890	25	735	43	948	16	939	87	971	66	856	22		
23.81	668	5	633	26	698	42	675	116	736	59	600	11	634	22
25.87	419	31	475	7	430	63	398	68	357	13	405	44	368	29
27.94	359	44	305	35	347	26	325	29	348	7	257	4.4	278	4
30.00	256	14	236	35	214	58	213	48	226	36	187	3.3	194	0.7
32.06	181	13	141	26	171	11	143	14	134	39	126	1.4	170	7.9
34.12	116	9	77	2	100	2	87	10	81	3.3	62	8.6	72	1.9
36.18	54	3	49	14	49	4	39	1.3	33	11	36	1.0	35	0.7
38.24	35	4	24	3	25	2	22	1.3	34	10	22	0.2	29	1.0
40.30	16	1	10.7	1.4	12.4	0.6	14	1.0	19	0.7	21	0.3	28	1.7
42.35	6.4	0.6	4.2	1.2	10	0.4	15	1.6	22	4.3	27	1.1	29	2.6
44.41	4.0	0.6	6.4	1.0	12.6	4	22	2	30	0.8	31	0.5	43	2.2
46.46	4.9	0.5	10.6	1.8	16	0.6	24	1	38	6	39	0.5		
48.51	11	1.2	18	2.6	22	0.4	33	2.5	44	8	40	0.8	51	0.9
50.56	18	0.7	27	3.9	31	3.5	43	3.4	50	3	48	2.1	55	2.6
52.60	25	0.7	29	3	34	1.4	49	4.3	54	45	55	1.0	56	2.8
54.65	31	1.6	38	2.5	35	2.6	54	3.4	49	1.3	56	1.1	57	2.5

TABLE II. POLARIZATIONS, ANGLES ARE IN DEGREES AND ENERGIES IN MEV.

$\theta_{c.m.}$ \ E_{LAB}	17.13	19.04	20.84	22.99	24.93	27.14	28.98
15.53	-.014±.004	-.034±.005	-.061±.005	-.043±.004	-.047±.004	-.03 ±.004	-.012±.004
17.60	-.032±.004	-.061±.005	-.07 ±.005	-.086±.006		-.051±.004	-.045±.004
19.67	-.055±.005	-.076±.004	-.096±.005	-.107±.006	-.085±.005	-.099±.005	-.098±.006
21.74	-.08 ±.006	-.133±.007	-.136±.007	-.111±.009	-.142±.007	-.129±.006	-.124±.007
23.81	-.097±.006	-.132±.007	-.204±.009	-.195±.011	-.172±.008	-.169±.009	-.155±.009
25.87	-.113±.006	-.163±.010	-.246±.014	-.269±.015	-.246±.011	-.213±.010	-.229±.013
27.94	-.125±.007	-.22 ±.010	-.251±.007	-.302±.015	-.313±.014	-.279±.013	-.264±.014
30.00		-.232±.011	-.325±.014	-.379±.017	-.382±.017	-.334±.015	-.331±.017
32.06	-.229±.010	-.251±.014	-.452±.023	-.429±.021	-.469±.019	-.406±.017	-.433±.021
34.12	-.259±.012	-.356±.017	-.547±.028	-.542±.024	-.614±.025	-.446±.019	-.448±.022
36.18	-.291±.014	-.51 ±.026	-.709±.045	-.718±.036	-.638±.026	-.543±.024	-.428±.022
38.24	-.335±.017	-.651±.028	-.878±.033	-.832±.034	-.673±.028	-.375±.019	-.187±.015
40.30	-.402±.02	-.774±.032	-.845±.035	-.575±.026	-.3 ±.02	-.011±.013	.139±.014
42.35	-.298±.025	-.394±.035	-.347±.025	-.042±.017	.134±.017	.234±.015	.169±.014
44.41	.526±.032	.444±.032	.244±.021	.268±.017	.33 ±.019	.305±.016	.328±.017
46.46	.72 ±.034	.453±.04	.295±.02	.295±.019	.286±.015	.278±.015	.322±.018
48.51	.494±.024	.319±.022	.274±.016	.262±.015		.25 ±.014	.247±.015
50.56	.329±.017	.267±.015	.228±.015	.223±.013	.221±.015	.205±.012	.203±.013
52.6	.211±.014	.19 ±.015	.192±.015	.17 ±.012	.145±.012	.159±.011	.147±.011
54.65	.157±.012	.145±.013	.162±.013	.133±.011	.132±.012	.12 ±.010	.114±.010

TABLE III. OPTICAL-MODEL PARAMETERS FOR BEST FITS

THE FOLLOWING PARAMETERS WERE HELD FIXED AT THE VALUES

r_o=1.17fm, r_i=1.33fm, r_{so}=.94fm, a_o=.65fm, a_i=a_{so}=.6fm

E_{LAB}	V	W	W_d	V_{so}	χ^2_σ	χ^2_p	χ^2_t/N
17.13	51.52	3.75	2.92	6.51	27	240	6.8
19.04	51.58	5.16	2.3	8.26	16	76	2.3
20.84	49.96	4.48	2.59	8.46	65	122	4.7
22.99	48.83	3.06	3.76	7.42	19	55	1.85
24.93	47.77	1.36	5.26	6.58	47	79	3.0
27.14	46.64	0.136	6.76	5.29	37	167	5.0
28.98	46.01	0.0	6.74	4.62	56	436	12.0

The last three columns contain the χ-squared of the cross sections, of the analyzing powers and the combined χ^2 per point respectively.

TABLE IV : OPTICAL MODEL PARAMETERS FOR BEST FITS WITH THE SPIN-ORBIT REAL DEPTH HELD FIXED ;
THE FOLLOWING PARAMETERS WERE HELD FIXED AT THE VALUES
r_o=1.17fm, r_i=1.33fm, r_{so}=.94fm, a_o=.65fm, a_i=a_{so}=.6fm

E_{LAB}	V	W	W_d	V_{so}	χ^2_σ	χ^2_p	χ^2_t/N
† 19.04	51.6	5.16	2.3	6.2	29	647	16.9
* 19.04	49.08	0.0	6.98	6.2	40	163	5.07
† 20.84	49.96	4.48	2.59	5.9	80	1107	29.67
* 20.84	47.83	0.0	6.22	5.9	84	529	15.33
† 22.99	48.83	3.06	3.76	5.6	26	461	12.17
* 22.99	47.78	0.0	6.26	5.6	36	270	7.65
† 24.93	47.76	1.36	5.26	5.3	51	329	9.5
* 24.93	47.37	0.0	6.51	5.3	54	273	8.17
† 27.14	46.64	0.136	6.76	4.9	39	206	6.12
* 27.14	46.64	0.136	6.76	4.9	39	206	6.12

† V_{SO} interpolated linearly between 17 and 29 MeV other parameters as in table III.

* V_{SO} interpolated linearly, other parameters adjusted to provide the best fit.

TABLE V - PHASE SHIFTS CORRESPONDING TO BEST-FIT OPTICAL MODEL PARAMETERS OF TABLE III, δ's ARE IN DEGREES

E_p	δ	η	δ	η	δ	η	δ	η	δ	η	δ	η	δ	η	δ	η	δ	η	δ	η	δ	η	δ	η
MeV	$s_{1/2}$		$p_{1/2}$		$p_{3/2}$		$d_{3/2}$		$d_{5/2}$		$f_{5/2}$		$f_{7/2}$		$g_{7/2}$		$g_{9/2}$		$h_{9/2}$		$h_{11/2}$		$i_{11/2}$		$i_{13/2}$	
17.13	62.6	0.51	22.0	0.39	38.6	0.44	149.9	0.52	174.0	0.45	121.8	0.24	154.9	0.61	11.1	0.72	15.6	0.44	2.3	0.95	3.2	0.94	0.50	0.99	0.63	0.99
19.04	55.6	0.56	14.6	0.36	34.4	0.42	143.8	0.46	176.0	0.39	112.4	0.24	155.8	0.58	14.4	0.64	11.2	0.18	3.3	0.93	5.2	0.90	0.77	0.99	1.1	0.98
20.84	45.1	0.47	4.1	0.40	24.1	0.45	137.2	0.48	171.1	0.42	103.8	0.29	151.2	0.60	17.6	0.57	-10.3	0.04	4.3	0.90	7.2	0.86	1.1	0.98	1.5	0.98
22.99	35.4	0.50	-2.5	0.45	14.2	0.49	134.5	0.49	165.7	0.45	104.4	0.38	144.7	0.58	22.5	0.43	62.9	0.10	5.8	0.84	9.5	0.77	1.6	0.96	2.2	0.96
24.93	27.2	0.54	-8.5	0.50	5.9	0.54	132.2	0.51	159.7	0.46	103.6	0.44	138.8	0.59	27.6	0.31	68.0	0.17	7.1	0.76	11.3	0.67	2.1	0.94	2.9	0.93
27.14	18.8	0.55	-14.2	0.53	-3.0	0.56	130.8	0.49	153.1	0.46	103.8	0.49	131.7	0.58	37.5	0.19	72.3	0.21	8.5	0.66	12.6	0.56	2.7	0.89	3.7	0.88
28.98	13.0	0.56	-18.6	0.56	-8.9	0.58	129.6	0.50	148.8	0.48	102.9	0.52	127.6	0.58	50.6	0.19	77.1	0.27	10.4	0.60	15.3	0.50	3.4	0.86	4.5	0.85

TABLE VI - PHASE SHIFTS CORRESPONDING TO OPTICAL MODEL PARAMETERS OF TABLE IV FOR V_{so} LINEARLY INTERPOLATED AND THE OTHER PARAMETERS ADJUSTED FOR THE BEST FIT TO THE DATA.

E_p	$s_{1/2}$		$p_{1/2}$		$p_{3/2}$		$d_{3/2}$		$d_{5/2}$		$f_{5/2}$		$f_{7/2}$		$g_{7/2}$		$g_{9/2}$		$h_{9/2}$		$h_{11/2}$		$i_{11/2}$		$i_{13/2}$	
MeV	δ	η	δ	η	δ	η	δ	η	δ	η	δ	η	δ	η	δ	η	δ	η	δ	η	δ	η	δ	η	δ	η
17.13	62.5	.50	22.0	.38	38.6	.43	149.9	0.52	174.0	0.45	121.8	0.24	154.9	0.61	11.1	0.72	15.6	0.44	2.3	0.95	3.2	0.94	0.50	0.99	0.63	0.99
19.04	47.4	.56	9.6	.42	24.6	.48	140.8	0.53	165.4	0.43	118.2	0.29	146.3	0.60	9.8	0.52	7.3	0.28	2.9	0.88	4.0	0.86	0.76	0.98	0.94	0.97
20.84	38.0	.59	0.57	.48	14.6	.53	136.7	0.56	161.0	0.48	109.3	0.36	140.9	0.62	14.6	0.45	15.2	0.14	4.0	0.86	5.6	0.82	1.1	0.97	1.4	0.96
22.99	31.5	.58	-3.88	.52	8.7	.55	135.6	0.54	158.9	0.48	108.0	0.44	137.8	0.61	20.7	0.34	-79.0	0.02	5.5	0.80	8.0	0.74	1.6	0.95	2.0	0.94
24.93	25.1	.57	-8.67	.53	2.8	.56	133.7	0.52	155.9	0.47	106.6	0.47	134.5	0.60	27.8	0.25	-73.6	0.12	6.9	0.73	10.0	0.66	2.1	0.92	2.7	0.92
27.14	20.6	.56	-11.8	.55	-1.4	.57	133.8	0.50	154.5	0.47	106.7	0.51	132.4	0.58	42.3	0.18	-71.9	0.23	8.9	0.65	13.0	0.56	2.8	0.89	3.6	0.88
28.98	13.0	.56	-18.6	.58	-8.9	.58	129.6	0.50	148.8	0.48	102.9	0.52	127.6	0.58	50.6	0.19	-77.1	0.27	10.4	0.60	15.3	0.50	3.4	0.86	4.5	0.85

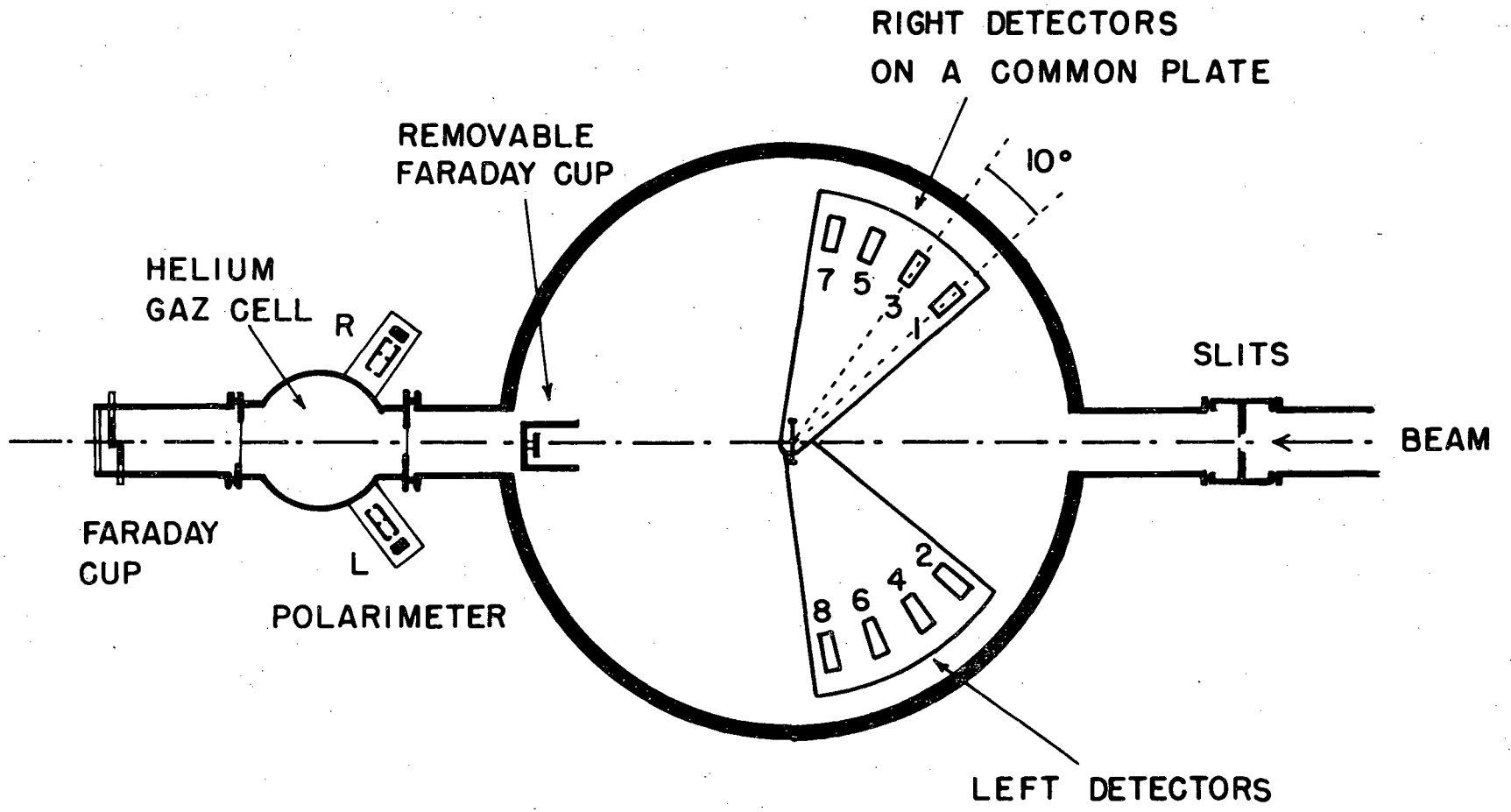
RIGHT DETECTORS
ON A COMMON PLATE
REMOVABLE
FARADAY CUP
10°
HELIUM
GAZ CELL
R
7 5 3 1
SLITS
BEAM
FARADAY
CUP
L
POLARIMETER
8 6 4 2
LEFT DETECTORS

Fig. 1

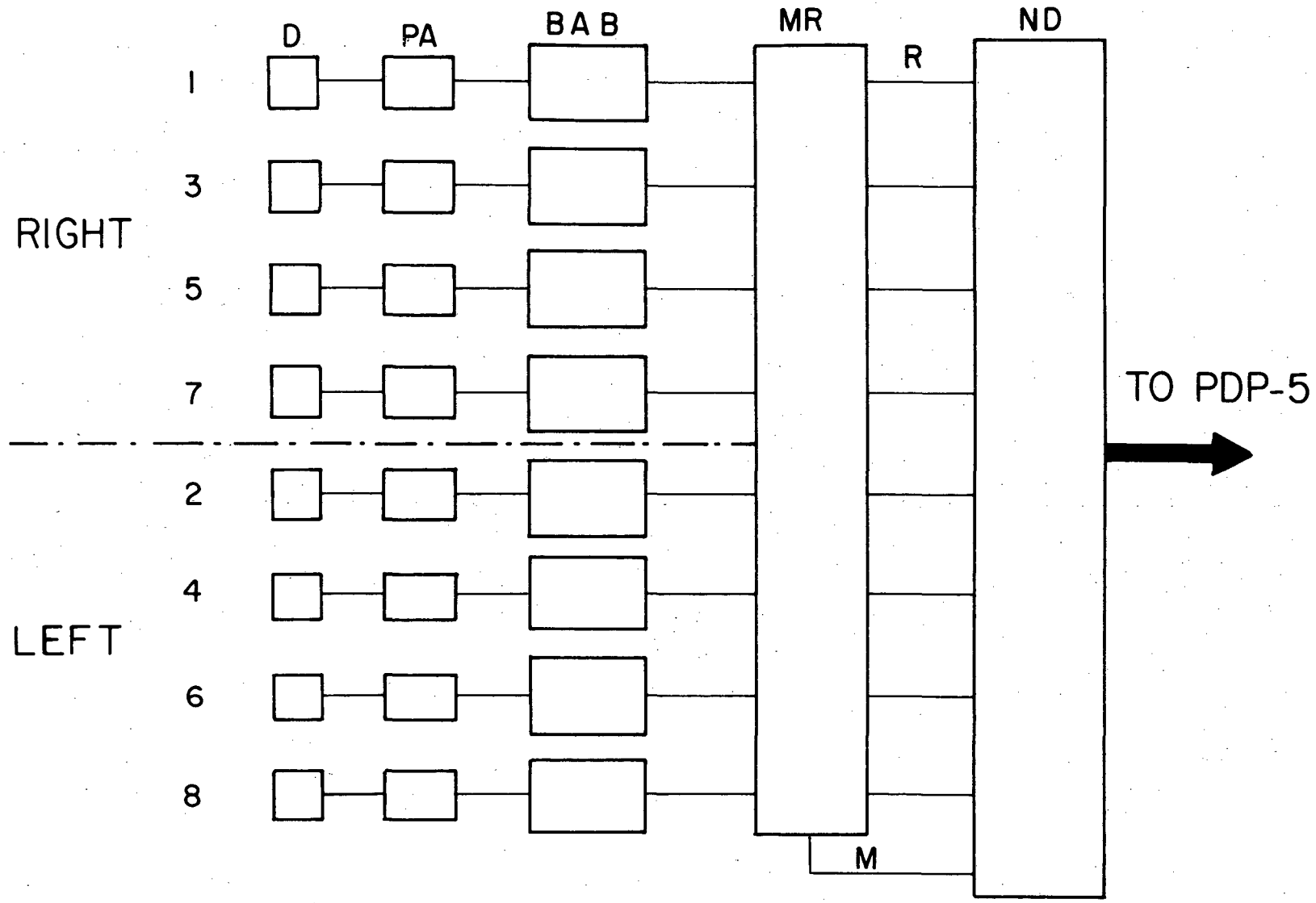

D: Detectors, PA: Preamplifiers, BAB: BERKELEY AMPLIFIER BOX, MR: 8 Channel mixer-router, R: Routing, M: Mixed output, ND: 4096 Ch. NUCLEAR DATA

Fig. 2

XBL 7812-13993

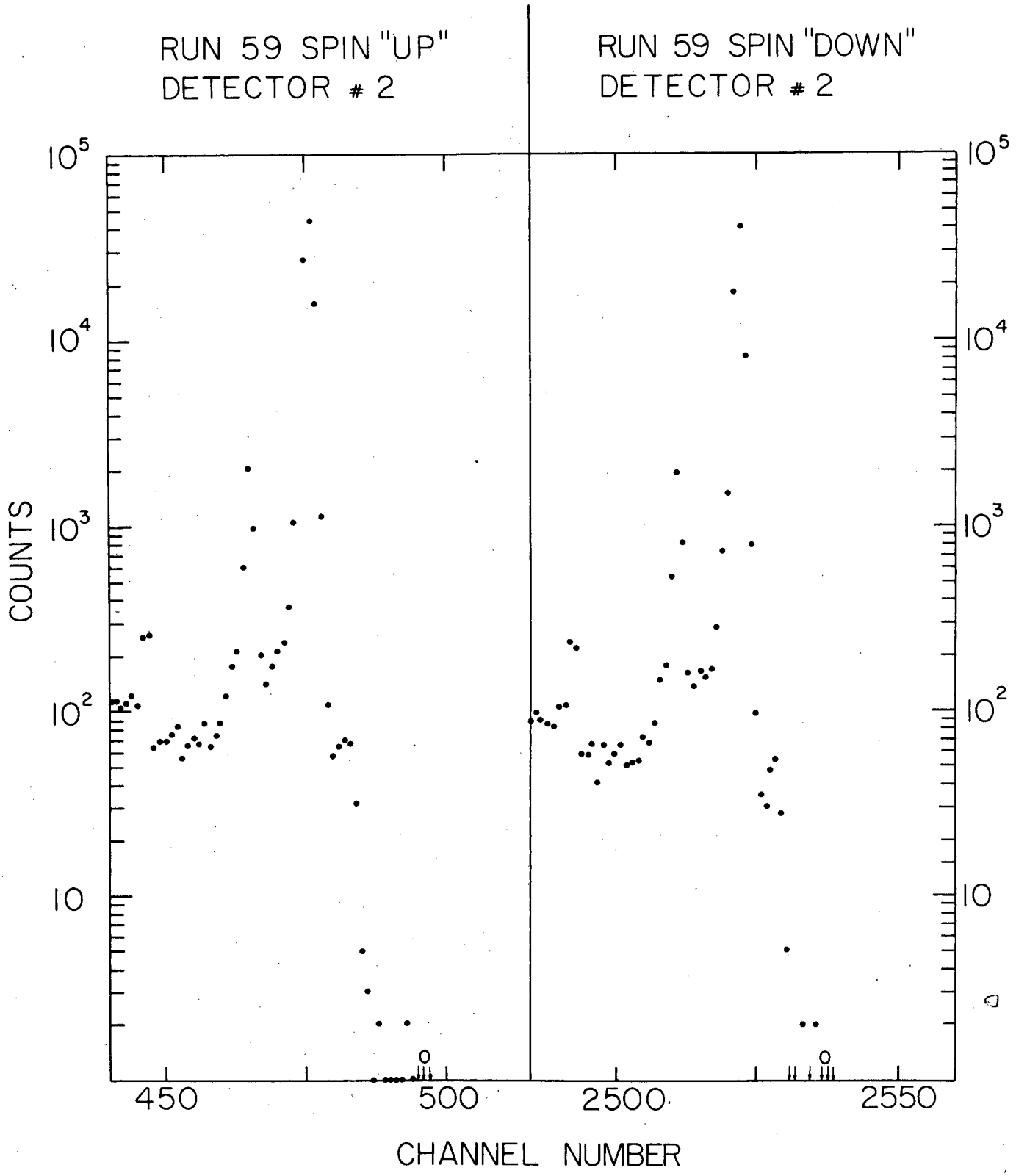

Fig. 3

XBL 7812-13992

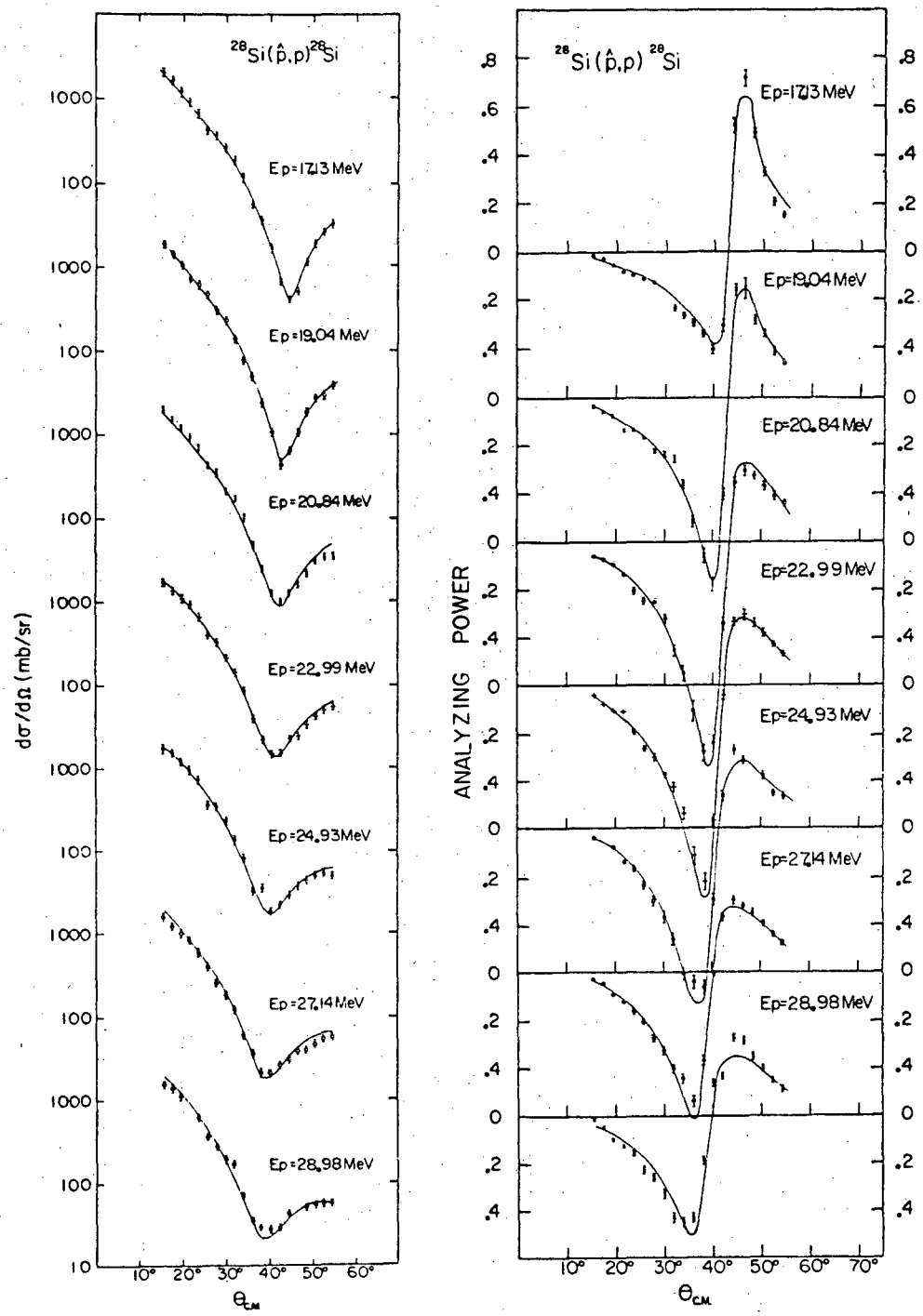

Fig. 4

XBL 788-2626

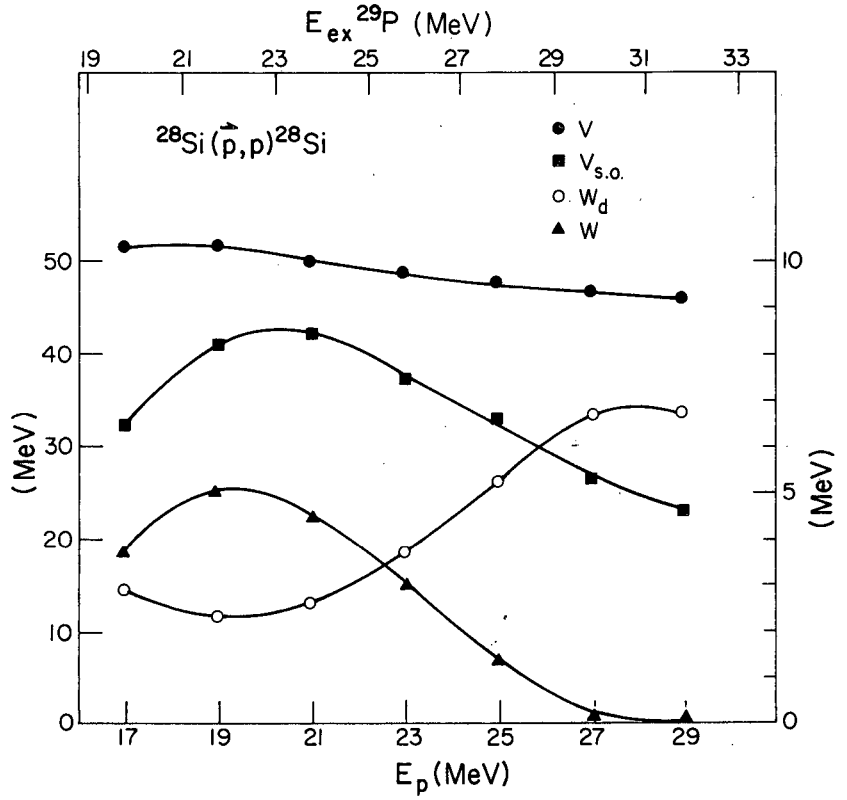
$E_{ex}{}^{29}P$ (MeV)
19
21
23
25
27
29
31
33
$^{28}Si(\vec{p},p)^{28}Si$
V
$V_{s.o.}$
W_d
W
50
40
30
20
10
0
(MeV)
10
5
0
(MeV)
17
19
21
23
25
27
29
E_p(MeV)
XBL 788-2627

Fig. 5

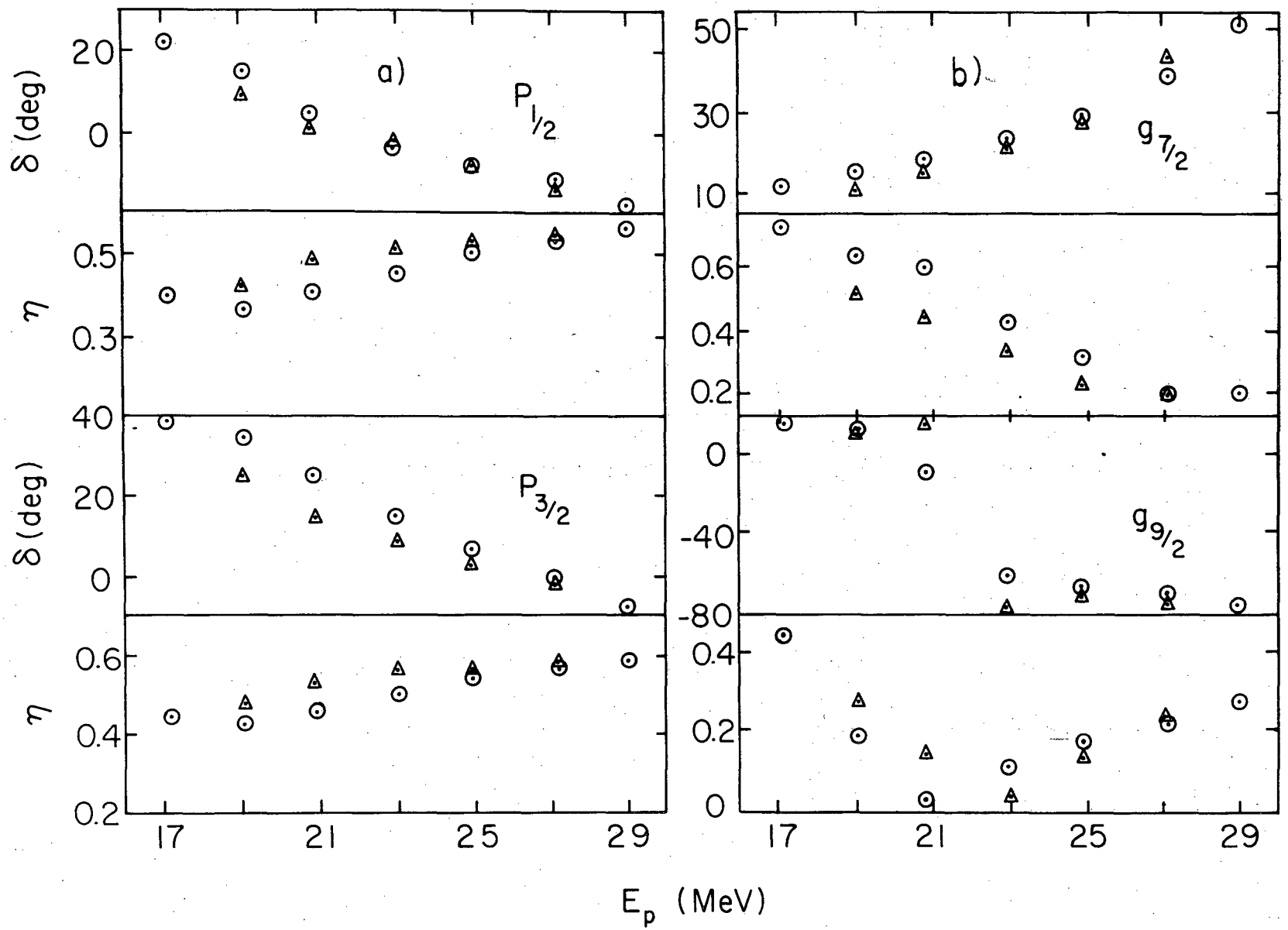

Fig. 6

XBL 7812-13990

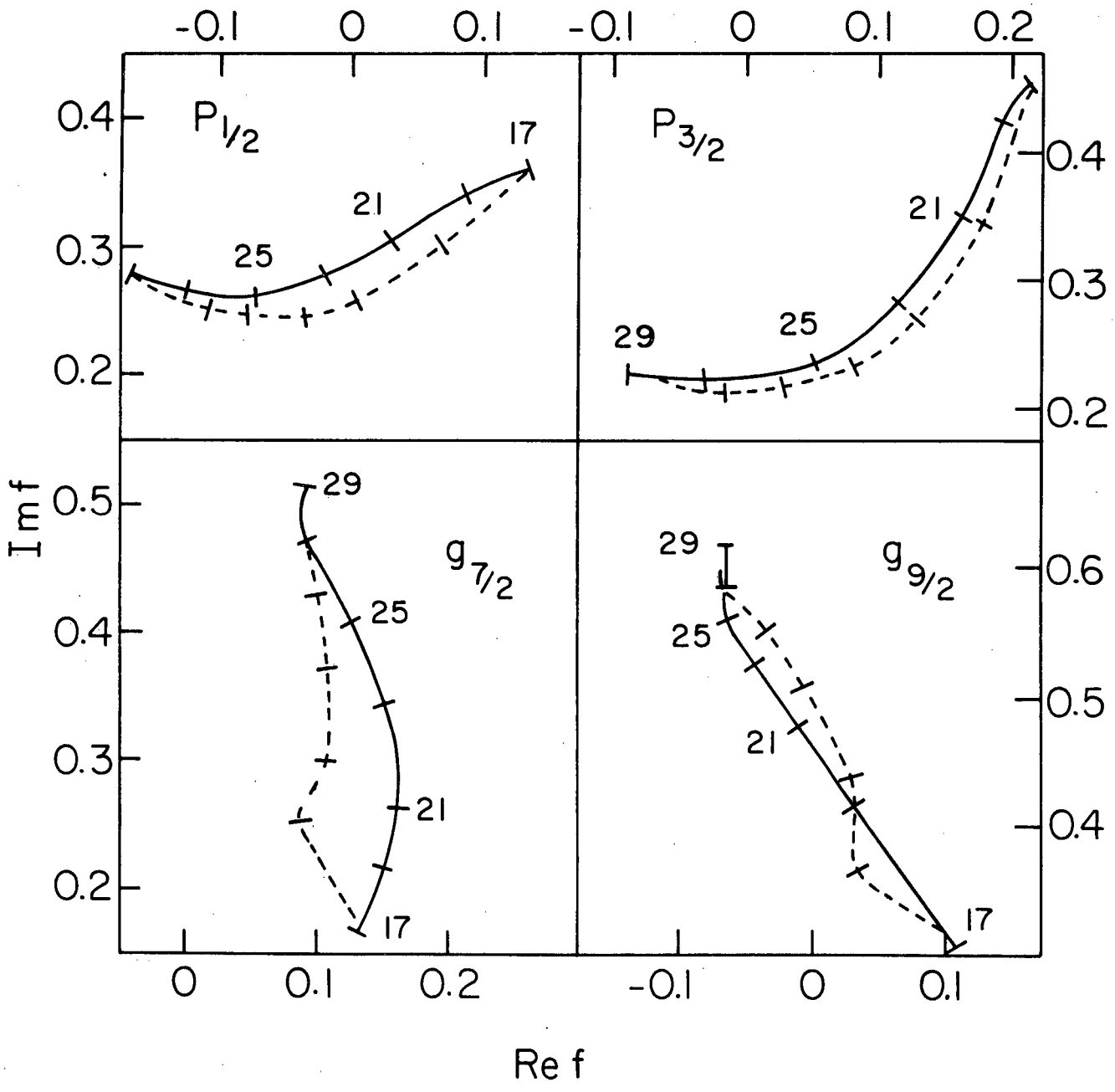

Fig. 7

XBL 7812-13991

This report was done with support from the Department of Energy. Any conclusions or opinions expressed in this report represent solely those of the author(s) and not necessarily those of The Regents of the University of California, the Lawrence Berkeley Laboratory or the Department of Energy.

TECHNICAL INFORMATION DEPARTMENT
LAWRENCE BERKELEY LABORATORY
UNIVERSITY OF CALIFORNIA
BERKELEY, CALIFORNIA 94720